7th International Symposium on

High-Temperature Metallurgical Processing

Characterization and Simulation of High Temperature Process

Session Chairs:
Baojun Zhao
Tarasankar DebRoy

HEAT AND FLUID FLOW MODELING TO EXAMINE 3D-PRINTABILITY OF ALLOYS

T. Mukherjee[1], J. S. Zuback[1], A. De[1] and T. DebRoy[1]

[1]Department of Materials Science and Engineering, The Pennsylvania State University,
University Park, PA, 16801, USA

Keywords: Additive manufacturing, Numerical modeling, 3D-Printability

Abstract

For successful commercial applications of additive manufacturing, metallic parts need to be defect free, structurally sound and reliable. However, additively manufactured metallic parts are susceptible to distortion, lack of fusion defects and compositional changes. Methods to measure susceptibilities of various alloys to these defects are needed but not currently available. Here we show that the necessary theories can be developed based on a well-tested numerical heat transfer and fluid flow model and decades of research in the field of welding. The proposed theories are validated with experimental results reported in the literature.

Introduction

Additive manufacturing (AM) of alloys offers many advantages over the conventional techniques for producing 'near-net-shape' parts. AM allows layer-by-layer fabrication of parts with complex geometries that are used for applications in medical, aerospace, automotive and many other industries [1,2]. However, thermal distortion, lack of inter-layer bonding due to inadequate fusion and loss of alloying elements from molten pool due to vaporization are major challenges in AM.

Thermal distortion in AM originates from non-uniform heating and cooling of the deposit. The thickness of layers deposited, dimensions and mechanical properties of substrate, selection of deposition path [2], deposition strategy [3], time delay between the deposition of successive layers [4], number of layers [5] and other AM variables influence the thermal distortion in AM. Lack of fusion defects originate from inadequate penetration of the molten pool into the substrate or previously deposited layer. Important variables such as thermo-physical properties of the alloy, characteristics of the heat source and processing parameters determine the depth of penetration of the molten pool when depositing a particular layer. Adequate penetration of the molten pool into the substrate or the previously deposited layer needs to be ensured to avoid this defect. During AM of alloys, high temperatures at the surface of the molten pool can result in pronounced vaporization of alloying elements [6]. With a small melt pool size and high surface area-to-volume ratio of the molten pool that are common in AM processing, significant change of composition of the parts can occur due to selective vaporization of volatile alloying elements from the molten pool at different rates. Changes in chemical composition affect both microstructure and mechanical properties [6].

Here we show how a numerical heat transfer and fluid flow model can be used to examine the propensity of the above mentioned three common defects during AM of metallic parts. Susceptibilities of various alloys to these defects are constructed based on these theories and tested using independent experimental data. The results presented here provide a quantitative basis for 3D printing of sound metallic parts.

Heat transfer and fluid flow model

The three dimensional transient heat transfer and fluid flow model used here solves the equations of conservation of mass, energy and momentum [1]. These equations are available in standard text books [7] and published literature [8,9]. The model computes temperature and velocity fields at various locations from AM process variables, such as the laser power, power density distribution, scanning speed, chemical composition, particle size, feed rate and thermo-physical properties of the alloy powder [1, 10]. In laser-assisted AM, a fraction of the laser beam

energy is transferred from the laser beam to the alloy powders and substrate. The energy is included in the energy conservation equation as a volumetric heat source, S_v as:

$$S_v = \frac{D\eta_a P}{\pi\left(r_{eff}^z\right)^2 h_d} \exp\left[-D\left(\frac{x^2 + y^2}{\left(r_{eff}^z\right)^2}\right) - \beta(z)\right] \tag{1}$$

where D is the power distribution factor, η_a is the laser absorption coefficient, P is the laser beam power, $\left(r_{eff}^z\right)$ refers to the radius of the laser beam at any plane at a distance z from the surface, h_d is the thickness of the material layer being deposited on the substrate, x and y are the co-ordinates from the axis of the laser beam on the surface and $\beta(z)$ is laser power attenuation coefficient. [11]

The heat input from the laser beam to the substrate or the previously deposited layer is considered as a surface heat flux, S_s, which is expressed as [12]:

$$S_s = \frac{D\eta\, P_{eff}}{\pi\left(r_{eff}\right)^2} \exp\left[-D\left(\frac{x^2 + y^2}{\left(r_{eff}\right)^2}\right)\right] \tag{2}$$

where P_{eff} is the available power on the surface, η is the laser absorption coefficient estimated using Bramson's equation [13] and r_{eff} is the effective radius of the laser beam at the substrate. The surface heat flux S_s is specified as a source term for the equation of conservation of energy at any surface. The laser power absorbed by the alloy powder depends on the absorptivity of the powder material. P_{eff} is the net power available that is utilized for the melting of the powder particles. The effective power P_{eff} can be expressed as $P_{eff} = P - P_L$ where, P_L is the total loss of the laser power.

The boundary conditions for the thermal analysis include heat exchange by convection and radiation with the surroundings. The boundary conditions for the velocities at the free surface are based on Marangoni convection. [1,8-9] The transient heat transfer and fluid flow calculations are performed for a solution domain representing the substrate, deposited layers, and the surrounding gas as shown in Figure 1.
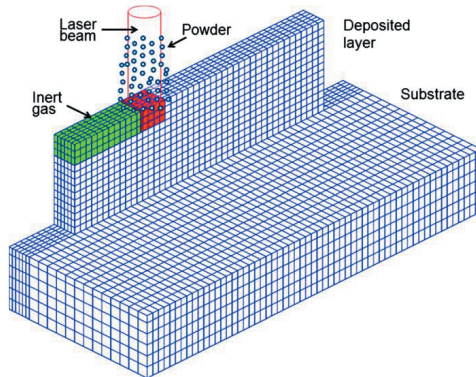
Figure 1. *Schematic representation of application of numerical model in the solution domain for AM process [1]*

The continuous movement of the laser beam is discretized using small shifts in the direction of scanning. The time-step for each shift of the laser beam is calculated from the deposition length and the laser scanning speed. An idle time is considered at the end of the simulation of each layer. The procedure is repeated until the simulation of all the layers is completed and calculations are continued until the specimen cools.

Table I. *Process conditions used in numerical calculations*

Parameter Set	Laser power (W)	Beam radius (mm)	Scanning speed (mm/s)	Layer thickness (mm)	Substrate thickness (mm)
1	2000	1.5	10.6	0.90	10
2	210	0.5	12.5	0.38	4
3	200	0.5	12.5	0.38	4

Figure 2 shows the computed melt pool geometry for the laser-based AM process of Ti-6Al-4V. Each color band in the profile represents a temperature range. The yellow colored regions in all the figures indicate that the deposited materials have reached at least the solidus temperature of the alloy. The molten pools are shown by red color. The vectors show the computed velocity fields in the molten region. A reference vector is shown by an arrow and a comparison of the length of this arrow with the vectors shown in the plots reveals the magnitudes of the computed velocities.
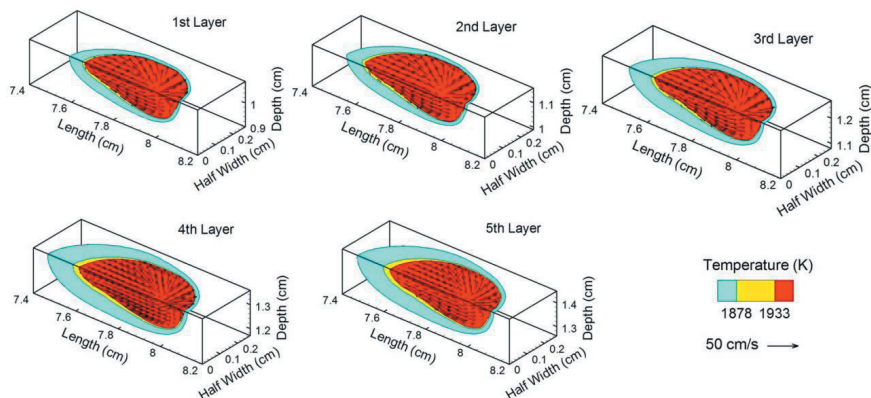
Figure 2. *Temperature and velocity fields at the middle of the built during laser based AM process of Ti-6Al-4V using process Parameter Set 1 in Table I.*

A fair agreement between the calculated build shape and size, and the corresponding measured build profile in Figure 3 indicates that the modeling results can be used to estimate thermal distortion, composition changes and lack of fusion defects with confidence.
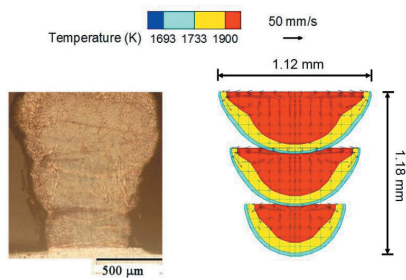
Figure 3. *Comparison between the numerically calculated and the corresponding actual build shape [1] with Parameter Set 2 of Table I.*

Thermal distortion

Thermal distortion in AM parts is caused by non-uniform expansion and contraction of different regions of the part that experience changes in temperature. Propensity for thermal distortion is calculated from the maximum thermal strain that largely depends on the molten pool dimensions. A larger pool size indicates a higher amount of contraction during solidification. Therefore, thermal strain increases with molten pool dimensions. Figure 4 shows experimentally measured maximum thermal strains (ε) reported in the literature [14-18] as a function of length of the molten pool (L). The lengths of the molten pools are calculated using the heat transfer and fluid flow model. The linear correlation between maximum thermal strain and molten pool length is given in Figure 4. Table II shows the estimated values of maximum thermal strains (ε) for various alloys using the linear correlation. Increasing layer thickness increases the thermal strain because of higher temperatures resulting from lower heat conduction from the molten pool into the substrate as shown in Table II. Thermal strain is the highest for Ti-6Al-4V, which can be attributed to its relatively low density and thermal diffusivity. The ranking of the alloys in Table II provides a relative scale of their printability considering their susceptibility to thermal distortion.
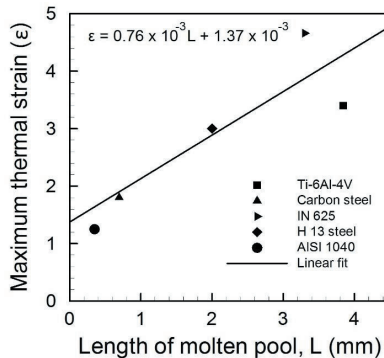
Figure 4. *Experimentally measured maximum thermal strain [14-18] as a function of length of the molten pool for five different alloys.*

475

Table II. *Values of maximum thermal strain (ε) in laser-based AM of a single-track three-layer deposition of SS 316, Ti6Al4V and IN 625 using Parameter Set 3 in Table I.*

Material	Layer no.	Maximum thermal strain
SS 316	1	2.4
	2	2.8
	3	3.1
Ti-6Al-4V	1	2.5
	2	2.9
	3	3.3
IN 625	1	1.8
	2	2.4
	3	2.5

Lack of fusion defects

In order to ensure appropriate inter-layer bonding, the melt pool in a deposited layer should exceed the layer thickness and adequately remelt the substrate or the previously deposited layer. Carroll et al. [19] reported a 99.999% dense part for direct energy deposition AM of Ti-6Al-4V, indicating proper inter-layer bonding. A corresponding depth was estimated about 1.02 mm for a layer thickness of 0.89 mm. This depth of penetration is about 15% higher than the layer thickness, which appears to be quite adequate for obtaining parts with near theoretical density.

The three-dimensional heat transfer and fluid flow model is used to estimate penetration depths for three alloys over a range of linear heat inputs. Table III shows that for a given heat input, Ti-6Al-4V will have the highest penetration depth (d), while SS 316 will have the lowest. Therefore, Ti-6Al-4V and SS 316 are the least and most susceptible to lack of fusion defects, respectively.

The results presented here provide a relative assessment of the susceptibilities of various alloys to lack of fusion defects. For alloys that are highly susceptible to lack of fusion defects, AM variables like laser power, scanning speed and powder feed rate should be appropriately adjusted to attain an adequate penetration depth.

Table III. *Computed penetration depth, (d), for three alloys using Parameter Set 3 in Table I.*

Heat input [J/mm]	SS 316 d [mm]	IN 625 d [mm]	Ti-6Al-4V d [mm]
16	0.384	0.445	0.479
20	0.426	0.479	0.517
24	0.452	0.502	0.551
28	0.467	0.521	0.574
32	0.483	0.540	0.597

Composition change

Temperatures and geometries of the molten pool are calculated using the three-dimensional heat transfer and fluid flow model. The equilibrium vapor pressures of all alloying elements are estimated from available thermodynamic data [20,21]. The vaporization fluxes of alloying elements, J_i, are estimated from the computed temperatures, T, vapor pressures, P_i, and the Langmuir equation:

$$J_i = \frac{\lambda P_i}{\sqrt{2\pi M_i T}} \tag{3}$$

where M_i is the molecular weight of element i, and λ is a positive fraction accounting for the condensation of some vaporized atoms. The surface area and volume of the molten pool are computed from the numerical heat transfer and fluid flow model. Table IV shows that Ti-6Al-4V and IN 625 will experience the most and least composition change, respectively.

Results for Ti-6Al-4V agree with results from Brice et al. [22], who reported an average composition change of approximately 0.9 wt% Al. Temperatures of the molten pool are higher for Ti-6Al-4V than the other alloys due to the relatively low thermal conductivity and density of the latter. A larger composition change for Ti-6Al-4V can be attributed to the higher temperatures and relatively high equilibrium vapor pressure of aluminum over the liquid alloy. For alloys highly susceptible to composition change, appropriate AM variables such as laser power density and scanning speed should be adjusted to reduce loss of volatile alloying elements.

Table IV. *Composition changes due to vaporization of constituting elements of three alloys during AM using the Langmuir equation (λ=0.05).*

Element	Al	Cr	Fe	Mn	Mo	Ni	Ti	V
Alloy	wt%	wt%	wt%	wt%	wt%	wt%	wt%	wt %
IN 625	−0.0008	−0.0117	−0.0002	-	0.00202	0.00984	4×10^{-5}	-
SS 316	-	0.0157	0.165	−0.220	-	0.0364	-	-
Ti-6Al-4V	−0.922	-	-	-	-	-	0.881	0.041

Conclusion

Numerical heat transfer and fluid flow calculations can provide useful information about the relative susceptibilities of various alloys to thermal distortion, loss of alloying elements and lack of fusion defects that can form during AM of metallic parts. The computed susceptibilities have been validated with independent experimental data. Results show that Ti-6Al-4V is most susceptible to thermal strain and composition change but least susceptible to lack of fusion defects. Stainless steel is more susceptible to lack of fusion defects than the other alloys considered. The results provide an understanding of the printability of various alloy powders under commonly used AM process conditions based on numerical heat transfer and fluid flow calculations.

References

[1] V. Manvatkar, A. De, and T. DebRoy, "Heat transfer and material flow during laser assisted multi-layer additive manufacturing," *Journal of Applied Physics* 116 (2014), 124905.

[2] P. Mercelis, and J. P. Kruth, "Residual stresses in selective laser sintering and selective laser melting," *Rapid Prototyping Journal* 12 (2006), 254.

[3] A. Nickel, D. Barnett, and F. Prinz, "Thermal stresses and deposition patterns in layered manufacturing," *Materials Science and Engineering: A,* 317 (2001), 59.

[4] R. Jendrzejewski, G. Sliwinski, and M. Krawczuk, "Investigation of temperature and stress fields in laser cladded coatings," *Applied Surface Science,* 254 (2007), 921.

[5] H. Pohl et al., "Thermal stresses in direct metal laser sintering," (Proceedings of the 12th Solid Freeform Fabrication Symposium, Austin, Texas, 2001).

[6] X. He, T. DebRoy, and P.W. Fuerschbach, "Alloying element vaporization during laser spot welding of stainless steel," *Journal of Physics D: Applied Physics,* 36 (2003), 3079.

[7] Patankar, S. V. *Numerical Heat Transfer and Fluid Flow* (New York, NY: McGraw-Hill 1982).

[8] T. DebRoy and S.A. David, "Physical processes in fusion welding," *Reviews of Modern Physics,* 67(1) (1995), 85-112.

[9] S.A. David and T. DebRoy, "Current issues and problems in welding science," *Science*, 257 (1992), 497-502.

[10] A. Raghavan et al. "Heat transfer and fluid flow in additive manufacturing," *Journal of Laser Applications,* 25(5) (2013), 1-8.

[11] A. Frenk et al. "Analysis of the laser-cladding process for stellite on steel," *Metallurgical and Materials Transactions B*, 28(3) (1997), 501-508.

[12] V. Neela and A. De, "Three dimensional heat transfer analysis of LENS™ process using finite element method," *The International Journal of Advanced Manufacturing Technology* 45(9-10) (2009), 935-943.

[13] W. M. Steen, *Laser Material Processing*, *2nd ed* (New York, NY: Springer-Verlag, 1998) 83.

[14] J. Grum and M. Znidarsie, "Microstructure, microhardness, and residual stress analysis of laser surface cladding of low-carbon steel," *Materials and Manufacturing Processes,* 19 (2004), 2.

[15] J.C. Heigel, P. Michaleris, and T.A. Palmer, "In situ monitoring and characterization of distortion during laser cladding of Inconel® 625," *Journal Materials Processing Technolology,* 220 (2015).

[16] P. Farahmand and R. Kovacevic, "An experimental–numerical investigation of heat distribution and stress field in single- and multi-track laser cladding by a high-power direct diode laser," *Optics and Laser Technology,* 63 (2014).

[17] S. Okano et al., "Effect of welding conditions on reduction in angular distortion by welding with trailing heat sink," *Science and Technology of Welding and Joining*, 17 (2012), 4.

[18] Y.P. Yang et al. "Material strength effect on weld shrinkage and distortion," *Welding Journal,* 93 (2014).

[19] B. E. Carroll, T. A. Palmer and A. M. Beese, "Anisotropic tensile behavior of Ti-6Al-4V components fabricated with directed energy deposition additive manufacturing," *Acta Materialia,* 87 (2015), 309-320.

[20] W.F. Gale and T.C. Totemeier. *Smithells Metals Reference Book, 8th edition* (Amsterdam, Boston: Elsevier Butterworth-Heinemann 2003)

[21] C.L. Yaws. *Handbook of Vapor Pressure*, (Houston: Gulf Pub. Co, 1994).

[22] C. A. Brice, et al. 4th International light metals technology conference. Broachbeach, QLD, Australia (2009).